Korean J. Chem. Eng., 33(12), 3473-3486 (2016)
DOI: 10.1007/s11814-016-0210-7

pISSN: 0256-1115
eISSN: 1975-7220

CO_2 absorption, density, viscosity and vapor pressure of aqueous potassium carbonate+2-methylpiperazine

Soung Hee Yun*, Young Eun Kim*, Jeong Ho Choi*, Sung Chan Nam*, Jaeeon Chang, and Yeo Il Yoon*,†**

*Green Energy Process Laboratory, Climate Change Research Division, Korea Institute of Energy Research, 152, Gajeong-ro, Yuseong-gu, Daejeon 34129, Korea
**Department of Chemical Engineering, University of Seoul, Siripdae-gil 13, Dongdaemun-gu, Seoul 02504, Korea
(*Received 25 March 2016 • accepted 18 July 2016*)

Abstract−The physical properties of the absorbent are important for designing a CO_2 capture process. The density and viscosity are used to calculate the mass transfer coefficient that determines the height of the absorber. Furthermore, these physical data affect the selection of liquid pump and pipe lines. Vapor pressure is a factor that estimates absorbent loss and condenser size. In this study, the physical properties of the aqueous potassium carbonate (K_2CO_3)+2-methylpiperazine (2MPZ) solution were obtained in a temperature range from 303.15 K to 343.15 K. The physical properties of the different aqueous K_2CO_3+2MPZ solutions (various amine concentrations and amounts of CO_2 absorbed) were measured to obtain the parameters for process design. A regression analysis was conducted for the experimental data. The densities of the aqueous K_2CO_3+2MPZ solutions increased when the amounts of absorbed CO_2 or 2MPZ concentrations were increased. The densities and viscosities of the absorbents decreased according to the increase in temperature. The viscosities of the absorbent increased when 2MPZ concentrations were increased. The temperature dependency of vapor pressure follows the Antoine equation; the CO_2 gas and aqueous solution of a base follows the vapor pressure variation of the mixed solution.

Keywords: KIERSOL, K_2CO_3, Carbon Dioxide, CO_2 Absorption, Density, Viscosity, Vapor Pressure, Regression Coefficient Parameters

INTRODUCTION

A wet-type CO_2 absorption process has advantages, including a low installation cost and large gas stream capacity. Alkanolamines such as monoethanolamine (MEA) and diethanolamine (DEA) are generally used in the absorption process because of their fast absorption rate, high CO_2 loading, and low raw material cost; however, these absorbents suffer from degradation, corrosion, foaming, and high regeneration energy [1]. Alkanolamines and potassium carbonate (K_2CO_3) solutions have been used for wet-type CO_2 absorption [2]. An aqueous K_2CO_3 solution has low regeneration energy, but its use is limited in coal-fired power plants because of the low solubility of K_2CO_3 solids in the water and a slow CO_2 absorption rate. A commercial scale plant, the Benfield process, is not suitable for CO_2 capture in coal-fired power plants because the process operates above 393.15 K. Therefore, it is necessary to develop a rate promoter of the aqueous K_2CO_3 solution to operate the CO_2 capture process at atmospheric pressure and room temperature [3-7]. Korea Institute of Energy Research (KIER) has developed a highly efficient CO_2 capture process, named KIERSOL™. KIERSOL is a K_2CO_3 based absorbent that has a low reboiler heat duty from 2.3 to 2.5 $GJ \cdot tCO_2^{-1}$ [8].

Process development goes through theoretical and experimental verification from laboratory to commercial scales. Although absorption performance shows excellent results in the lab scale tests, the operating cost of the process can be increased in the process due to physical and chemical properties of the absorbents. Therefore, it is essential to obtain the physical property data of the absorbent at the operating condition.

Density and viscosity data are necessary for the design of liquid pumps and heat exchangers [9,10]. The density of the absorbent is used to calculate the ratio between the liquid flow and the gas flow (L/G ratio). The density of the absorbent must be measured at various conditions because the values are changed according to the temperature and amount of absorbed CO_2. High viscosity causes drawbacks such as bubble generation and increasing pipe diameter and pump output.

Flooding velocity can be functionalized by liquid and gas rate, density and viscosity of the two fluids, and the characteristics of the packing material. Fluid density and liquid viscosity may affect flooding velocity in packed columns especially [11]. The model equations of transport property using density, viscosity and surface tension data are necessary for predicting liquid holdup, pressure drop and mass transfer correlations of process. Density and viscosity of solution are two major parameters for liquid film mass transfer coefficient estimation [12]. It is important that the mass transfer coefficients in the wetted area can be used for designing of absorption and desorption columns with packing [13]. Choi et al. [14] studied

†To whom correspondence should be addressed.
E-mail: 21yoon@kier.re.kr
‡This article is dedicated to Prof. Sung Hyun Kim on the occasion of his retirement from Korea University.

mass transfer between the CO_2 and the aqueous 2-methylpiperidine solution. Mass transfer coefficients were calculated using experimental density and viscosity values [14].

A stripper of the typical wet-type absorption process was elevated to temperatures ranging from 373.15 to 393.15 K. Selection of an absorbent with low vapor pressure was recommended to minimize the absorbent loss in the stripper. Gorset et al. [15] reported the results of the process operation using MEA and Aker solutions S21 and S26 (S21, S26: absorbent brand) [15]. They operated the process for 10,000-hrs, and ~96-236·10^6 Sm^3 gas was treated. The amount of absorbent loss for MEA, S21, and S26 was 2.6, 0.6, and 0.3 kg amine·ton CO_2^{-1}, respectively. The amount of absorbent loss is directly related to the volatility and vapor pressure [16]. Therefore, the vapor pressure of the absorbent can be used to evaluate the amount of absorbent produced and to calculate the operating cost [17,18]. The vapor pressure is a thermodynamically important factor in the process design [19].

In this study, the physical properties of the absorbents (K_2CO_3 and various 2MPZ concentrations solutions) and the CO_2 loaded absorbents (various CO_2 loading) were measured to obtain the parameters for process design.

REACTION MECHANISM

1. Potassium Carbonate Mechanism

The overall chemical reaction of the aqueous K_2CO_3 solution and CO_2 is as follows [20,21]:

$$K_2CO_3+H_2O+CO_2 \leftrightarrow 2KHCO_3 \quad (1)$$

Because K_2CO_3 and $KHCO_3$ (potassium bicarbonate) are strong electrolytes, it can be assumed that potassium is shown only in the form of K^+ ions and can therefore be expressed as shown in Eq. (2):

$$CO_3^{2-}+H_2O+CO_2 \leftrightarrow 2HCO_3^- \quad (2)$$

The overall reaction proceeds according to Eqs. (3) and (4):

$$CO_3^{2-}+H_2O \leftrightarrow HCO_3^-+OH^- \quad (3)$$

$$CO_2+OH^- \leftrightarrow HCO_3^- \quad (4)$$

Eq. (3) can be explained by the reaction of Astarita et al. [22]. The principal mechanisms shown in Eqs. (5) and (6) are a direct reaction of dissolved CO_2 with OH^- at a pH>10 [22].

$$CO_2+OH^- \leftrightarrow HCO_3^- \text{ (fast)} \quad (5)$$

$$HCO_3^-+OH^- \leftrightarrow CO_3^{2-}+H_2O \text{ (instantaneous)} \quad (6)$$

At pH<8, the predominant mechanism is direct hydration of dissolved CO_2:

$$CO_2+H_2O \leftrightarrow H_2CO_3 \text{ (slow)} \quad (7)$$

$$H_2CO_3+OH^- \leftrightarrow HCO_3^-+H_2O \text{ (instantaneous)} \quad (8)$$

Fresh absorbent (CO_2 non-loaded absorbent) is shown at a pH> 10 according to Eqs. (5) and (6). The measured value of absorbent that is used in the experiment is shown in Table 1. The hydrogen exponent was measured using Horiba's Minivap VPXpert.

Table 1. Hydrogen exponent of the absorbents at T=313.15 K

Concentration of the aqueous absorbents/wt%		pH
Absorbent	Promoter	
K_2CO_3 15.0	2MPZ 1.0	11.75
	2MPZ 3.0	11.98
	2MPZ 5.0	12.14
	2MPZ 7.0	12.24
	2MPZ 7.5	12.29
	2MPZ 10.0	12.51

2. Promoted Potassium Carbonate Mechanism

The CO_2 reaction mechanism of promoted K_2CO_3 solution can be explained by Eqs. (9) and (10). The mechanism is as follows [22]:

$$CO_2+H_2AsO_3^- \leftrightarrow \text{Intermediate} \quad (9)$$

$$\text{Intermediate}+OH^- \leftrightarrow HCO_3^-+H_2AsO_3^- \quad (10)$$

For the case of an amine with a lone pair, Eqs. (11) and (12) show the reaction:

$$CO_2+RR'NH \leftrightarrow RR'NCOOH \quad (11)$$

$$RR'NCOOH+OH^- \leftrightarrow HCO_3^-+RR'NH \quad (12)$$

where, R and R′ mean different alkyl groups, respectively.

Eqs. (9)-(10) and Eqs. (11)-(12) are not chemically different; consequently, Eqs. (13) and (14) are shown in the following general case:

$$CO_2+\text{Promoter} \leftrightarrow \text{Intermediate} \quad (13)$$

$$\text{Intermediate}+OH^- \leftrightarrow HCO_3^-+\text{Promoter} \quad (14)$$

Each reaction is divided into a homogeneous catalysis and shuttle mechanism. Eq. (13) in a homogeneous catalysis reaction is so much faster than Eq. (14) that it immediately and locally follows. However, Eq. (14) in the shuttle mechanism is so much slower that it takes place in the bulk of the liquid.

EXPERIMENT

The reagents, MEA (purity 99.0%, Sigma Aldrich), 2-methylpiperazine (2MPZ, purity 98.0%, Sigma Aldrich) and K_2CO_3 (purity 99.5%, Samchun chemicals), were used in preparing the absorbents without further purification.

The CO_2-loaded absorbents were taken up from continuous stirred tank reactor (CSTR) experiments. The CSTR apparatus consists of a reactor with a 500 mL internal volume.

The outlet gas was analyzed by gas chromatography (GC, 7890A from Agilent) to calculate the CO_2 concentration. Fig. 1 shows the experimental setup for CSTR. The GC was equipped with a porapak-Q column (6 ft·1/8 in) (from Supelco Co.) and a thermal conductivity detector (TCD). Column oven and detector temperatures were maintained at 393 K and 523 K, respectively.

CO_2 and N_2 mixture gas (CO_2 30 vol%, N_2 balance) at a rate of 500 ml·min^{-1} was supplied into the reactor using a Special Gas Co. gas. A bubbler type gas injector and an agitator were used to maximize contact between the gas and the absorbent. A condenser was

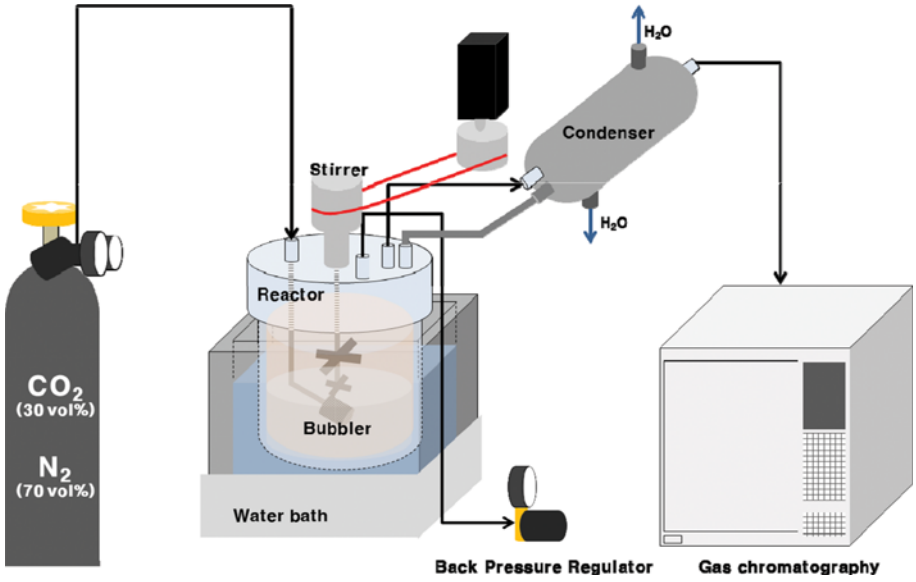

Fig. 1. Schematic of continuous stirred tank reactor (CSTR).

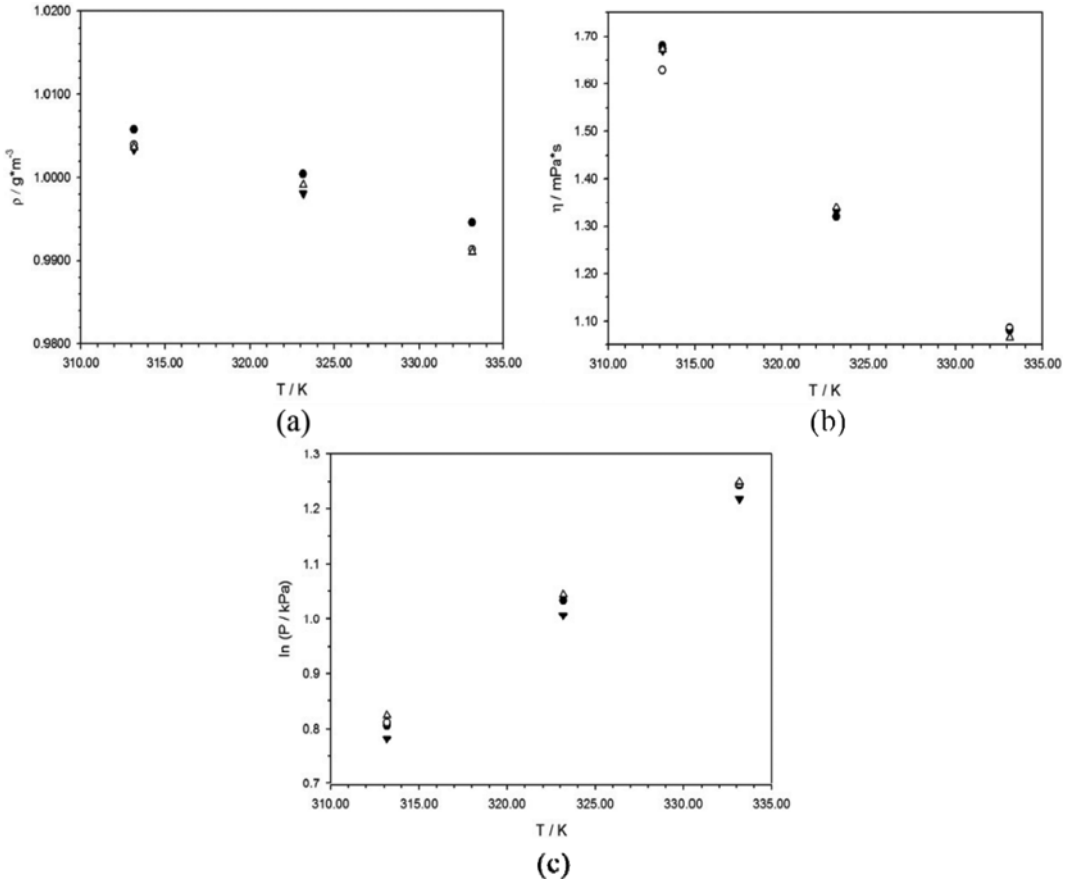

Fig. 2. Physical properties according to temperature of MEA 30 wt%+water 70 wt%; (a) density; ●, this work; ○, data of Maham et al. [24]; ▼, data of Amundsen et al. [9]; △, data of Han et al. [23]; (b) viscosity; ●, this work; ○, data of Maham et al. [25]; ▼, data of Amundsen et al. [9]; △, data of Arachchige et al. [26]; (c) vapor pressure; ●, this work; ○, data of Kim et al. [28]; ▼, data of Belabbaci et al. [27]; △, data of Wu et al. [29].

installed in the top of the reactor to prevent absorbent loss. Temperature and pressure of the reactor were measured with K-type thermocouples and a pressure sensor (M5126 from Sensys Co.).

The amount of absorbed CO_2 in the absorbent (n_{abs,CO_2}) was cal-

culated from Eq. (15):

$$n_{abs,\,CO_2} = \frac{(P_{CO_2,\,in} \cdot V_{CO_2,\,in}) - (P_{CO_2,\,out} \cdot V_{CO_2,\,out})}{RT} \quad (15)$$

where $P_{CO_2,in}$ and $V_{CO_2,in}$ are the inlet partial pressure and volume of CO_2, respectively, and $P_{CO_2,out}$ and $V_{CO_2,out}$ are outlet partial pressure and volume. R and T are the gas constant and temperature.

The CO_2 loading (α) represents the amount of dissolved CO_2 in the absorbent defined as the molar ration between CO_2 and the solute in the absorbent (K_2CO_3 and/or amine) (Eq. (16)).

$$CO_2\ \text{loading} = \alpha = n_{abs,\,CO_2} \cdot n_{solute}^{-1} \quad (16)$$

Densities of the pure absorbents and CO_2-loaded absorbents were measured by using a densimeter (DM40 from Mettler Toledo Co.) with a ±0.0001 g·cm^{-3} limit of error. Commercial aqueous MEA 30 wt% solution was evaluated to confirm the repeatability of this experimental apparatus because the properties of this solution have not been studied and reported. Fig. 2(a) shows the comparison of densities between measured values and reference values [9,23,24]. Repeatability of this apparatus was good, as deviation between measured value (1.0057 g·cm^{-3}) and reference values (1.0034-1.0040 g·cm^{-3}) was ± 0.0023 at 313.15 K.

The viscosities were measured with a viscosity meter (DV-II+ pro from Brookfield Co.) with ±1.0% accuracy and ±0.2% repeatability. The replacement of the spindle in the viscometer is possible in accordance with the viscosity of the fluid. A suitable spindle (CPE-40) with a 0.2-3000.0 mPa·s range of viscosity was selected in the measurement because pure absorbents and CO_2-loaded absorbents exhibited viscosity values between 0.5 and 5.0 mPa·s. Fig. 2(b) shows the comparison of viscosities between measured values and reference values [9,25,26]. Average deviation of aqueous MEA 30 wt% solution was ±0.05 between measured value (1.68 mPa·s) and reference values (1.63-1.67 mPa·s) at 313.15 K.

The vapor pressure was measured using a Minivap VPXpert apparatus from Grabner instruments with ±0.4% repeatability and ±1.0% reproducibility. The vapor pressure values had good agreement with the reference values in Fig. 2(c) [27-29]. Average deviation of aqueous MEA 30 wt% solution was ±0.35 between measured value (6.40 kPa) and reference values (6.05-6.67 kPa) at 313.15 K.

RESULTS AND DISCUSSION

1. Selection of Absorbent Concentration

Phase behavior should be considered in the K_2CO_3 based absorbent for CO_2 capture. The aqueous K_2CO_3 solution reacts with CO_2 and forms $KHCO_3$ with three-times less solubility in water than K_2CO_3. Therefore, solubility of $KHCO_3$ in water at the operating temperature determines the application of the absorbent concentration. $KHCO_3$ solid salt causes serious problems such as pipe closing [30]. Solubility data regarding $KHCO_3$ in water have been reported by researchers in experimental conditions. The aqueous K_2CO_3 solution formed $KHCO_3$ solid salt at 300.15 K or less [31]. Tosh et al. (1974) investigated equilibrium vapor pressures for 20% and 30% equivalent K_2CO_3 solutions as a function of conversion to $KHCO_3$ and found that equilibrium vapor pressures of these absorbents were practically the same [31].

Kim et al. [32] measured CO_2 loadings of PZ or 2MPZ promoted aqueous K_2CO_3 solutions. They found that K_2CO_3 20.0 wt%+PZ or 2MPZ 10.0 wt% formed $KHCO_3$ solid salts [32]; therefore, the absorbent concentrations could not be used in a conventional absorption process.

2MPZ promoted in an aqueous K_2CO_3 solution is a promising absorbent with a high CO_2 loading and low absorption heat [33]. In this study, the physical properties of the aqueous K_2CO_3+2MPZ solutions were obtained because the data were not sufficient for process design. The physical properties of aqueous K_2CO_3 15.0 wt%+2MPZ 7.5 or 10.0 wt% solutions were measured at various temperatures. The promoter concentrations of 1.0, 3.0, 5.0, and 7.0 wt% were added to an aqueous K_2CO_3 15.0 wt% solution to study the effect of the promoter concentration to the physical properties.

2. CO_2 Loading of Absorbent

CO_2 loadings of aqueous K_2CO_3+2MPZ solutions were measured at 313.15 K, and the CO_2-loaded absorbents were collected for physical property measurements. CO_2 absorption curves and CO_2 loadings are shown in Fig. 3 and Table 2. CO_2 loadings of the absorbents were limited to 0.8 mol CO_2·mol solute^{-1}.

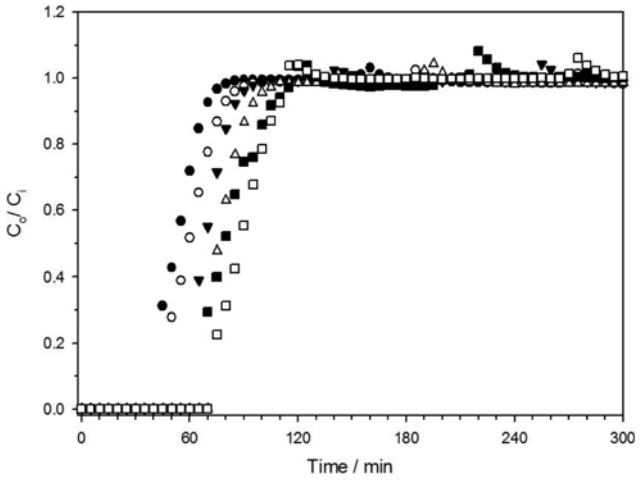

Fig. 3. CO_2 absorption breakthrough curve of aqueous K_2CO_3+2MPZ at T=313.15 K, P=1.15 bar. ●, K_2CO_3 15.0 wt%+2MPZ 1.0 wt%; ○, K_2CO_3 15.0 wt%+2MPZ 3.0 wt%; ▼, K_2CO_3 15.0 wt%+2MPZ 5.0 wt%; △, K_2CO_3 15.0 wt%+2MPZ 7.0 wt%; ■, K_2CO_3 15.0 wt%+2MPZ 7.5 wt%; □, K_2CO_3 15.0 wt%+2MPZ 10.0 wt%.

Table 2. CO_2 loading of the absorbents at T=313.15 K and P=1.15 bar

Concentration of the aqueous absorbents/wt%		CO_2 loading (mol CO^2·mol solute^{-1})
Absorbent	Promoter	
K_2CO_3 15.0	2MPZ 1.0	0.79
	2MPZ 3.0	0.80
	2MPZ 5.0	0.78
	2MPZ 7.0	0.80
	2MPZ 7.5	0.74
	2MPZ 10.0	0.71

Table 3. Experimental densities (ρ) for the CO_2-loaded aqueous K_2CO_3+2MPZ (wt%)

α/mol CO_2·mol solute^{-1}	ρ/g·cm^{-3} (SD)				
	303.15 K	313.15 K	323.15 K	333.15 K	343.15 K
			K_2CO_3 15.0 wt%+2MPZ 1.0 wt%		
0.00	1.1312 (0.0000)	1.1267 (0. 0000)	1.1217 (0.0000)	1.1164 (0.0000)	1.1113 (0.0000)
0.22	1.1335 (0.0000)	1.1287 (0. 0000)	1.1234 (0.0000)	1.1179 (0.0000)	1.1122 (0.0000)
0.43	1.1363 (0.0000)	1.1314 (0.0000)	1.1262 (0.0000)	1.1206 (0.0000)	1.1149 (0.0000)
0.64	1.1385 (0.0000)	1.1336 (0.0000)	1.1284 (0.0000)	1.1228 (0.0000)	1.1171 (0.0000)
0.79	1.1420 (0.0000)	1.1372 (0.0000)	1.1320 (0.0000)	1.1264 (0.0000)	-
			K_2CO_3 15.0 wt%+2MPZ 3.0 wt%		
0.00	1.1308 (0.0000)	1.1263 (0.0000)	1.1212 (0.0000)	1.1159 (0.0000)	1.1107 (0.0000)
0.25	1.1377 (0.0000)	1.1327 (0.0000)	1.1272 (0.0000)	1.1214 (0.0000)	1.1153 (0.0000)
0.44	1.1415 (0.0000)	1.1364 (0.0000)	1.1309 (0.0000)	1.1250 (0.0000)	1.1188 (0.0000)
0.62	1.1442 (0.0000)	1.1392 (0.0000)	1.1337 (0.0000)	1.1279 (0.0000)	1.1212 (0.0000)
0.80	1.1492 (0.0000)	1.1443 (0.0000)	1.1388 (0.0000)	1.1331 (0.0000)	-
			K_2CO_3 15.0 wt%+2MPZ 5.0 wt%		
0.00	1.1307 (0.0000)	1.1260 (0.0000)	1.1208 (0.0000)	1.1155 (0.0000)	1.1099 (0.0000)
0.22	1.1393 (0.0000)	1.1341 (0.0000)	1.1285 (0.0000)	1.1225 (0.0000)	1.1162 (0.0000)
0.43	1.1461 (0.0000)	1.1408 (0.0000)	1.1350 (0.0000)	1.1289 (0.0000)	1.1225 (0.0000)
0.65	1.1508 (0.0000)	1.1457 (0.0000)	1.1401 (0.0000)	1.1341 (0.0000)	1.1279 (0.0000)
0.78	1.1565 (0.0000)	1.1514 (0.0000)	1.1459 (0.0000)	1.1399 (0.0000)	-
			K_2CO_3 15.0 wt%+2MPZ 7.0 wt%		
0.00	1.1305 (0.0000)	1.1258 (0.0000)	1.1205 (0.0000)	1.1150 (0.0000)	1.1093 (0.0000)
0.24	1.1424 (0.0000)	1.1369 (0.0000)	1.1312 (0.0000)	1.1250 (0.0000)	1.1186 (0.0000)
0.44	1.1507 (0.0000)	1.1452 (0.0000)	1.1393 (0.0000)	1.1330 (0.0000)	1.1264 (0.0000)
0.63	1.1565 (0.0000)	1.1511 (0.0000)	1.1454 (0.0000)	1.1393 (0.0000)	1.1329 (0.0000)
0.80	1.1625 (0.0000)	1.1574 (0.0000)	1.1518 (0.0000)	1.1458 (0.0000)	-
			K_2CO_3 15.0 wt%+2MPZ 7.5 wt%		
0.00	1.1305 (0.0000)	1.1259 (0.0000)	1.1206 (0.0000)	1.1150 (0.0000)	1.1092 (0.0000)
0.23	1.1459 (0.0000)	1.1381 (0.0000)	1.1323 (0.0000)	1.1262 (0.0000)	1.1197 (0.0000)
0.41	1.1520 (0.0000)	1.1464 (0.0000)	1.1405 (0.0000)	1.1342 (0.0000)	1.1276 (0.0000)
0.63	1.1594 (0.0000)	1.1541 (0.0000)	1.1484 (0.0000)	1.1423 (0.0000)	1.1360 (0.0000)
0.74	1.1634 (0.0000)	1.1581 (0.0000)	1.1525 (0.0000)	1.1464 (0.0000)	-
			K_2CO_3 15.0 wt%+2MPZ 10.0 wt%		
0.00	1.1304 (0.0000)	1.1257 (0.0000)	1.1202 (0.0000)	1.1144 (0.0000)	1.1085 (0.0000)
0.20	1.1443 (0.0000)	1.1388 (0.0000)	1.1330 (0.0000)	1.1268 (0.0000)	1.1203 (0.0000)
0.40	1.1569 (0.0000)	1.1512 (0.0000)	1.1451 (0.0000)	1.1386 (0.0000)	1.1319 (0.0000)
0.60	1.1660 (0.0000)	1.1606 (0.0000)	1.1546 (0.0000)	1.1483 (0.0000)	1.1419 (0.0000)
0.71	1.1713 (0.0000)	1.1659 (0.0000)	1.1602 (0.0000)	1.1540 (0.0000)	-

3. Density

The densities of the pure and CO_2-loaded absorbents were measured three times for each sample. The standard deviations (SD) of the measurements were calculated by Eq. (17) and presented in Table 3.

$$SD = \sqrt{\frac{1}{n}\sum_{i=1}^{n}(x_i - \bar{x})^2} \quad (17)$$

where x_i, $\bar{x}$, and n are the observed value, mean value of the observations, and number of data, respectively.

All data from the density measurements showed high repeatability (SD=0.0000). The density data of aqueous K_2CO_3+2MPZ measured at 343.15 K was inaccurate. Specifically, the densities of the CO_2-loaded absorbents with high CO_2 loading (above CO_2 loading=0.7) at 343.15 K were not presented in Table 3 because of the low accuracy. CO_2 stripping occurred at a relatively high temperature in the stripper [34]. Accurate values were not obtained because gas bubbles rise at a rapid rate from CO_2-loaded K_2CO_3+2MPZ solutions at the elevated temperature.

Relations between density and temperature are presented as 1st-order, 2nd-order and 3rd-order polynomial functions [35-41]. The regression equation is as shown in Eq. (18).

$$\rho/g\cdot cm^{-3} = A_0 + A_1(T/K) + A_2(T/K)^2 + A_3(T/K)^3 \quad (18)$$
(constant absorbent concentration)

The regression coefficient parameters in Eq. (18) are presented

Table 4. Regressed parameters of density (ρ) for temperature used in Eq. (18)

α/mol CO_2·mol solute^{-1}	Regression coefficient parameters					
	A_0	A_1	A_2	A_3	R^2	SEE
			K_2CO_3 15.0 wt%+2MPZ 1.0 wt%			
0.00	$-7.90388\cdot10^{-1}$	$1.84463\cdot10^{-2}$	$-5.76231\cdot10^{-5}$	$5.83337\cdot10^{-8}$	1.0000	0.0000
0.22	$3.05910\cdot10^{-1}$	$8.21287\cdot10^{-3}$	$-2.56653\cdot10^{-5}$	$2.50005\cdot10^{-8}$	1.0000	0.0000
0.43	$5.89590\cdot10^{-1}$	$5.60306\cdot10^{-3}$	$-1.75865\cdot10^{-5}$	$1.66671\cdot10^{-8}$	1.0000	0.0000
0.64	$5.91790\cdot10^{-1}$	$5.60306\cdot10^{-3}$	$-1.75865\cdot10^{-5}$	$1.66671\cdot10^{-8}$	1.0000	0.0000
0.79	1.09765	$7.52600\cdot10^{-4}$	$-2.00000\cdot10^{-6}$	$3.68951\cdot10^{-20}$	1.0000	0.0000
			K_2CO_3 15.0 wt%+2MPZ 3.0 wt%			
0.00	$-7.96696\cdot10^{-1}$	$1.84874\cdot10^{-2}$	$-5.76945\cdot10^{-5}$	$5.83337\cdot10^{-8}$	1.0000	0.0000
0.25	$5.61424\cdot10^{-1}$	$5.80888\cdot10^{-3}$	$-1.79437\cdot10^{-5}$	$1.66672\cdot10^{-8}$	1.0000	0.0000
0.44	$8.40196\cdot10^{-1}$	$3.24024\cdot10^{-3}$	$-9.93638\cdot10^{-6}$	$8.33385\cdot10^{-9}$	1.0000	0.0000
0.62	2.16411	$-9.29600\cdot10^{-3}$	$2.96716\cdot10^{-5}$	$-3.33327\cdot10^{-8}$	1.0000	0.0000
0.80	−1.03219	$2.09648\cdot10^{-2}$	$-6.56300\cdot10^{-5}$	$6.66667\cdot10^{-8}$	1.0000	0.0000
			K_2CO_3 15.0 wt%+2MPZ 5.0 wt%			
0.00	$5.86889\cdot10^{-1}$	$5.57188\cdot10^{-3}$	$-1.75151\cdot10^{-5}$	$1.66671\cdot10^{-8}$	1.0000	0.0000
0.22	$8.41027\cdot10^{-1}$	$3.23025\cdot10^{-3}$	$-9.93639\cdot10^{-6}$	$8.33386\cdot10^{-9}$	1.0000	0.0000
0.43	$5.78918\cdot10^{-1}$	$5.77889\cdot10^{-3}$	$-1.79437\cdot10^{-5}$	$1.66672\cdot10^{-8}$	1.0000	0.0000
0.65	$2.90746\cdot10^{-1}$	$8.44987\cdot10^{-3}$	$-2.60939\cdot10^{-5}$	$2.50005\cdot10^{-8}$	1.0000	0.0000
0.78	1.63253	$-4.17888\cdot10^{-3}$	$1.36575\cdot10^{-5}$	$-1.66667\cdot10^{-8}$	1.0000	0.0000
			K_2CO_3 15.0 wt%+2MPZ 7.0 wt%			
0.00	$7.15923\cdot10^{-3}$	$1.09150\cdot10^{-2}$	$-3.38869\cdot10^{-5}$	$3.33338\cdot10^{-8}$	1.0000	0.0000
0.24	1.15185	$4.66940\cdot10^{-4}$	$-1.64337\cdot10^{-6}$	$5.38475\cdot10^{-13}$	1.0000	0.0000
0.44	$8.61521\cdot10^{-1}$	$3.20025\cdot10^{-3}$	$-9.93641\cdot10^{-6}$	$8.33388\cdot10^{-9}$	1.0000	0.0000
0.63	1.15701	$5.18103\cdot10^{-4}$	$-1.71479\cdot10^{-6}$	$5.34888\cdot10^{-13}$	1.0000	0.0000
0.80	$5.68493\cdot10^{-1}$	$5.93223\cdot10^{-3}$	$-1.81575\cdot10^{-5}$	$1.66667\cdot10^{-8}$	1.0000	0.0000
			K_2CO_3 15.0 wt%+2MPZ 7.5 wt%			
0.00	$-3.09370\cdot10^{-1}$	$1.37506\cdot10^{-2}$	$-4.23228\cdot10^{-5}$	$4.16671\cdot10^{-8}$	1.0000	0.0000
0.23	8.23851	$-6.42921\cdot10^{-2}$	$1.95532\cdot10^{-4}$	$-1.99999\cdot10^{-7}$	0.9998	0.0003
0.41	1.15857	$4.98108\cdot10^{-4}$	$-1.71481\cdot10^{-6}$	$5.49587\cdot10^{-13}$	1.0000	0.0000
0.63	$5.98127\cdot10^{-1}$	$5.73773\cdot10^{-3}$	$-1.78723\cdot10^{-5}$	$1.66672\cdot10^{-8}$	1.0000	0.0000
0.74	2.20424	$-9.40851\cdot10^{-3}$	$2.98150\cdot10^{-5}$	$-3.33333\cdot10^{-8}$	1.0000	0.0000
			K_2CO_3 15.0 wt%+2MPZ 10.0 wt%			
0.00	$-8.65189\cdot10^{-1}$	$1.89503\cdot10^{-2}$	$-5.84803\cdot10^{-5}$	$5.83338\cdot10^{-8}$	1.0000	0.0000
0.20	1.14784	$5.08105\cdot10^{-4}$	$-1.71480\cdot10^{-6}$	$5.48310\cdot10^{-13}$	1.0000	0.0000
0.40	$6.07752\cdot10^{-1}$	$5.69774\cdot10^{-3}$	$-1.78723\cdot10^{-5}$	$1.66672\cdot10^{-8}$	1.0000	0.0000
0.60	$-2.22932\cdot10^{-1}$	$1.34960\cdot10^{-2}$	$-4.20371\cdot10^{-5}$	$4.16672\cdot10^{-8}$	1.0000	0.0000
0.71	2.21517	$-9.41851\cdot10^{-3}$	$2.98150\cdot10^{-5}$	$-3.33333\cdot10^{-8}$	1.0000	0.0000

in Table 4.

The R^2 (R square) and standard error of the estimate (SEE) that are calculated using Eqs. (19) and (23) are also shown in Table 4.

$$R^2 = SSR \cdot SST^{-1} = 1 - (SSE \cdot SST^{-1}) \tag{19}$$

$$SST = \sum_{i=1}^{n} (x_i - \bar{x})^2 \tag{20}$$

$$SSR = \sum_{i=1}^{n} (\hat{x}_i - \bar{x})^2 \tag{21}$$

$$SSE = \sum_{i=1}^{n} (x_i - \hat{x}_i)^2 \tag{22}$$

$$SEE = \sqrt{\frac{SSE}{n-2}} = \sqrt{\frac{1}{n-2}\sum_{i=1}^{n} (x_i - \hat{x}_i)^2} \tag{23}$$

where SST, SSR, SST and $\hat{x}$ are the sum of the square total, sum of the square regression, sum of the square error, and predicted value, respectively. The R square and SEE indicate the suitability of the observed value and the regressed value. The R squares and SEEs of the predicted values from the observed values are within an acceptable error range.

A K_2CO_3 15.0 wt%+2MPZ 10.0 wt% graph at each CO_2 loading of the densities according to temperature increases is presented in Fig. 4 of the supporting information. The regression coefficient parameters led to an inference value from the density of the absor-

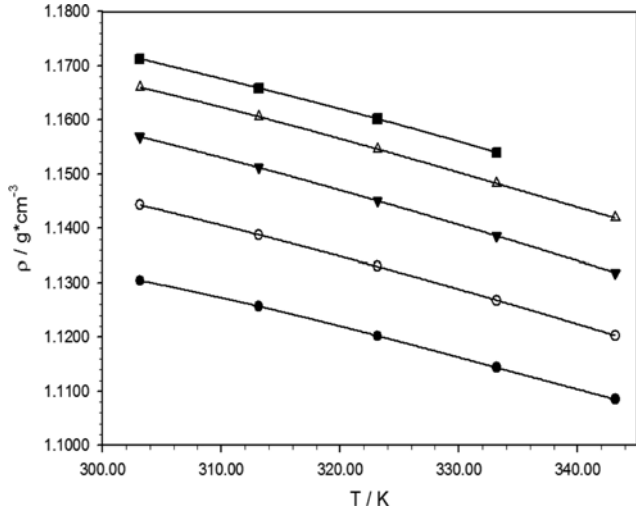

Fig. 4. Density according to temperature of K_2CO_3 15.0 wt%+2MPZ 10.0 wt%; ●, α=0; ○, α=0.20; ▼, α=0.40; △, α=0.60; ■, α=0.71; solid line, regression curve.

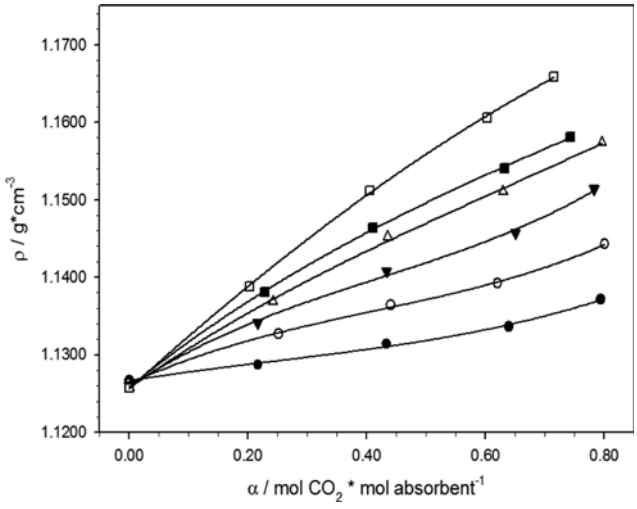

Fig. 5. Density according to CO_2 loading of 313.15 K; ●, K_2CO_3 15.0 wt%+2MPZ 1.0 wt%; ○, K_2CO_3 15.0 wt%+2MPZ 3.0 wt%; ▼, K_2CO_3 15.0 wt%+2MPZ 5.0 wt%; △, K_2CO_3 15.0 wt%+2MPZ 7.0 wt%; ■, K_2CO_3 15.0 wt%+2MPZ 7.5 wt%; □, K_2CO_3 15.0 wt%+2MPZ 10.0 wt%; solid line, regression curve.

bent, and are used as the data of the process design. Relationships between the density and CO_2 loading are presented as a 3rd-order polynomial function (Eq. (18)).

$$\rho/\text{g·cm}^{-3}=B_0+B_1(\alpha/\text{CO}_2\ \text{mol·amine mol}^{-1}) +B_2(\alpha/\text{CO}_2\ \text{mol·amine mol}^{-1})^2 +B_3(\alpha/\text{CO}_2\ \text{mol·amine mol}^{-1})^3\ \text{(constant temperature)} \quad (24)$$

The regression coefficient parameters are presented in Table 5. The R squares indicated the high suitability with the observed value, and SEEs are changed from four decimal points. The density value according to the 2MPZ concentration can be calculated by Eq. (24). The density graph according to CO_2 loading at 313.15 K was

Table 5. Regressed parameters of density (ρ) for CO_2 loading used in Eq. (24)

K_2CO_3+2MPZ/ wt%	Regression coefficient parameters					
	B_0	B_1	B_2	B_3	R^2	SEE
			303.15 K			
15.0+1.0	1.13115	$1.41214\cdot10^{-2}$	$-1.44768\cdot10^{-2}$	$1.73057\cdot10^{-2}$	0.9966	0.0005
15.0+3.0	1.13077	$3.87156\cdot10^{-2}$	$-5.17619\cdot10^{-2}$	$4.00422\cdot10^{-2}$	0.9991	0.0004
15.0+5.0	1.13061	$5.44454\cdot10^{-2}$	$-6.96662\cdot10^{-2}$	$5.36904\cdot10^{-2}$	0.9979	0.0009
15.0+7.0	1.13045	$5.89185\cdot10^{-2}$	$-3.97839\cdot10^{-2}$	$2.03661\cdot10^{-2}$	0.9994	0.0006
15.0+7.5	1.13057	$8.78759\cdot10^{-2}$	$-1.12961\cdot10^{-1}$	$7.12198\cdot10^{-2}$	0.9990	0.0008
15.0+10.0	1.13035	$7.57525\cdot10^{-2}$	$-2.90203\cdot10^{-2}$	$4.06654\cdot10^{-3}$	0.9997	0.0006
			313.15 K			
15.0+1.0	1.12665	$1.23359\cdot10^{-2}$	$-1.23388\cdot10^{-2}$	$1.68423\cdot10^{-2}$	0.9961	0.0005
15.0+3.0	1.12627	$3.54545\cdot10^{-2}$	$-4.62222\cdot10^{-2}$	$3.74339\cdot10^{-2}$	0.9992	0.0004
15.0+5.0	1.12592	$5.04388\cdot10^{-2}$	$-6.13196\cdot10^{-2}$	$4.87467\cdot10^{-2}$	0.9981	0.0009
15.0+7.0	1.12574	$5.38178\cdot10^{-2}$	$-3.07485\cdot10^{-2}$	$1.62617\cdot10^{-2}$	0.9992	0.0007
15.0+7.5	1.12587	$6.15424\cdot10^{-2}$	$-3.51802\cdot10^{-2}$	$1.42482\cdot10^{-2}$	0.9998	0.0003
15.0+10.0	1.12565	$6.90487\cdot10^{-2}$	$-1.46992\cdot10^{-2}$	$-4.72441\cdot10^{-3}$	0.9998	0.0005
			323.15 K			
15.0+1.0	1.12164	$1.00191\cdot10^{-2}$	$-6.45475\cdot10^{-3}$	$1.26971\cdot10^{-2}$	0.9951	0.0006
15.0+3.0	1.12117	$3.27659\cdot10^{-2}$	$-4.07913\cdot10^{-2}$	$3.40620\cdot10^{-2}$	0.9990	0.0004
15.0+5.0	1.12072	$4.76043\cdot10^{-2}$	$-5.72624\cdot10^{-2}$	$4.75834\cdot10^{-2}$	0.9984	0.0008
15.0+7.0	1.12045	$5.10704\cdot10^{-2}$	$-2.67155\cdot10^{-2}$	$1.49523\cdot10^{-2}$	0.9994	0.0006
15.0+7.5	1.12058	$5.79485\cdot10^{-2}$	$-2.86509\cdot10^{-2}$	$1.12527\cdot10^{-2}$	0.9999	0.0003
15.0+10.0	1.12016	$6.80018\cdot10^{-2}$	$-1.84384\cdot10^{-2}$	$2.01661\cdot10^{-3}$	0.9998	0.0005

Table 5. Continued

K_2CO_3+2MPZ/ wt%	Regression coefficient parameters					
	B_0	B_1	B_2	B_3	R^2	SEE
			333.15 K			
15.0+1.0	1.11634	$8.72304\cdot10^{-3}$	$-4.69820\cdot10^{-3}$	$1.19433\cdot10^{-2}$	0.9950	0.0006
15.0+3.0	1.11587	$2.95048\cdot10^{-2}$	$-3.52516\cdot10^{-2}$	$3.14537\cdot10^{-2}$	0.9991	0.0004
15.0+5.0	1.11542	$4.24021\cdot10^{-2}$	$-4.67591\cdot10^{-2}$	$4.11950\cdot10^{-2}$	0.9983	0.0008
15.0+7.0	1.11495	$4.60613\cdot10^{-2}$	$-1.70114\cdot10^{-2}$	$9.68153\cdot10^{-3}$	0.9994	0.0006
15.0+7.5	1.11498	$5.42489\cdot10^{-2}$	$-2.21782\cdot10^{-2}$	$8.06165\cdot10^{-3}$	0.9999	0.0002
15.0+10.0	1.11437	$6.52662\cdot10^{-2}$	$-1.59762\cdot10^{-2}$	$2.87353\cdot10^{-3}$	0.9999	0.0004
			343.15K			
15.0+1.0	1.11130	$-3.42691\cdot10^{-3}$	$4.28868\cdot10^{-2}$	$-3.64885\cdot10^{-2}$	1.0000	0.0000
15.0+3.0	1.11070	$1.55014\cdot10^{-2}$	$1.70785\cdot10^{-2}$	$-2.38152\cdot10^{-2}$	1.0000	0.0000
15.0+5.0	1.10990	$2.78933\cdot10^{-2}$	$8.71239\cdot10^{-3}$	$-1.39265\cdot10^{-2}$	1.0000	0.0000
15.0+7.0	1.10930	$3.37465\cdot10^{-2}$	$2.77065\cdot10^{-2}$	$-3.45224\cdot10^{-2}$	1.0000	0.0000
15.0+7.5	1.10920	$4.66150\cdot10^{-2}$	$7.09194\cdot10^{-6}$	$-1.04703\cdot10^{-2}$	1.0000	0.0000
15.0+10.0	1.10850	$5.68233\cdot10^{-2}$	$1.21676\cdot10^{-2}$	$-2.40591\cdot10^{-2}$	1.0000	0.0000

Table 6. Experimental viscosity (η) for the CO_2-loaded aqueous K_2CO_3+2MPZ (wt%)

α/mol CO_2· mol solute^{-1}	η/mPa·s (SD)				
	303.15 K	313.15 K	323.15 K	333.15 K	343.15 K
		K_2CO_3 15.0 wt%+2MPZ 1.0 wt%			
0.00	1.31 (0.02)	1.06 (0.02)	0.91 (0.02)	0.80 (0.01)	0.70 (0.01)
0.22	1.25 (0.01)	1.06 (0.01)	0.89 (0.01)	0.79 (0.01)	0.69 (0.02)
0.43	1.25 (0.01)	1.05 (0.00)	0.90 (0.01)	0.77 (0.01)	0.69 (0.02)
0.64	1.24 (0.01)	1.03 (0.01)	0.88 (0.01)	0.76 (0.01)	0.70 (0.01)
0.79	1.23 (0.01)	1.04 (0.03)	0.89 (0.01)	0.78 (0.01)	-
		K_2CO_3 15.0 wt%+2MPZ 3.0 wt%			
0.00	1.44 (0.00)	1.17 (0.02)	1.01 (0.02)	0.85 (0.03)	0.77 (0.01)
0.25	1.42 (0.01)	1.17 (0.01)	0.98 (0.01)	0.86 (0.01)	0.76 (0.00)
0.44	1.40 (0.01)	1.17 (0.01)	0.99 (0.01)	0.85 (0.01)	0.76 (0.01)
0.62	1.37 (0.01)	1.17 (0.01)	0.98 (0.01)	0.84 (0.02)	0.76 (0.01)
0.80	1.39 (0.00)	1.17 (0.01)	0.99 (0.01)	0.86 (0.02)	-
		K_2CO_3 15.0 wt%+2MPZ 5.0 wt%			
0.00	1.61 (0.02)	1.32 (0.02)	1.13 (0.03)	0.96 (0.02)	0.84 (0.03)
0.22	1.62 (0.01)	1.30 (0.01)	1.11 (0.02)	0.93 (0.01)	0.83 (0.01)
0.43	1.59 (0.00)	1.29 (0.00)	1.09 (0.01)	0.94 (0.01)	0.83 (0.02)
0.65	1.57 (0.01)	1.28 (0.01)	1.10 (0.01)	0.95 (0.02)	0.85 (0.01)
0.78	1.58 (0.01)	1.31 (0.00)	1.11 (0.01)	0.97 (0.01)	-
		K_2CO_3 15.0 wt%+2MPZ 7.0 wt%			
0.00	1.83 (0.01)	1.47 (0.02)	1.26 (0.03)	1.06 (0.05)	0.90 (0.04)
0.24	1.81 (0.04)	1.45 (0.03)	1.25 (0.03)	1.06 (0.03)	0.92 (0.02)
0.44	1.83 (0.03)	1.48 (0.02)	1.25 (0.01)	1.04 (0.01)	0.92 (0.01)
0.63	1.83 (0.01)	1.46 (0.01)	1.24 (0.01)	1.05 (0.01)	0.93 (0.03)
0.80	1.84 (0.01)	1.49 (0.01)	1.26 (0.01)	1.08 (0.02)	-
		K_2CO_3 15.0 wt%+2MPZ 7.5 wt%			
0.00	1.90 (0.05)	1.54 (0.01)	1.31 (0.01)	1.09 (0.04)	0.92 (0.03)
0.23	1.91 (0.01)	1.53 (0.01)	1.25 (0.02)	1.08 (0.01)	0.93 (0.02)
0.41	1.89 (0.01)	1.51 (0.02)	1.26 (0.03)	1.09 (0.03)	0.95 (0.02)
0.63	1.90 (0.01)	1.53 (0.01)	1.29 (0.02)	1.11 (0.03)	0.96 (0.03)
0.74	1.91 (0.01)	1.54 (0.01)	1.33 (0.04)	1.13 (0.04)	-

Table 6. Continued

α/mol CO_2·mol solute^{-1}	η/mPa·s (SD)				
	303.15 K	313.15 K	323.15 K	333.15 K	343.15 K
			K_2CO_3 15.0 wt%+2MPZ 10.0 wt%		
0.00	2.34 (0.01)	1.85 (0.03)	1.52 (0.04)	1.30 (0.02)	1.12 (0.03)
0.20	2.29 (0.01)	1.79 (0.00)	1.46 (0.01)	1.26 (0.02)	1.07 (0.03)
0.40	2.26 (0.01)	1.80 (0.01)	1.50 (0.01)	1.28 (0.01)	1.11 (0.01)
0.60	2.29 (0.00)	1.82 (0.01)	1.52 (0.02)	1.29 (0.01)	1.12 (0.02)
0.71	2.32 (0.02)	1.87 (0.02)	1.55 (0.04)	1.31 (0.02)	-

Table 7. Regressed parameters of viscosity (η) for temperature used in Eq. (25)

α/mol CO_2·mol solute^{-1}	Regression coefficient parameters				
	C_0	C_1	C_2	R^2	SEE
			K_2CO_3 15.0 wt%+2MPZ 1.0 wt%		
0.00	−1.47584	$1.27220\cdot10^2$	$-2.30235\cdot10^2$	0.9982	0.01
0.22	−2.77554	$4.86204\cdot10^2$	$-1.41110\cdot10^2$	0.9988	0.01
0.43	−2.64298	$4.32912\cdot10^2$	$-1.52193\cdot10^2$	0.9992	0.01
0.64	−1.52861	$1.39491\cdot10^2$	$-2.23282\cdot10^2$	0.9983	0.01
0.79	−2.64853	$4.49864\cdot10^2$	$-1.45644\cdot10^2$	0.9999	0.00
			K_2CO_3 15.0 wt%+2MPZ 3.0 wt%		
0.00	−1.81231	$2.13025\cdot10^2$	$-2.05273\cdot10^2$	0.9978	0.02
0.25	−1.81647	$2.13740\cdot10^2$	$-2.04578\cdot10^2$	0.9997	0.01
0.44	−2.29730	$3.44208\cdot10^2$	$-1.72586\cdot10^2$	0.9994	0.01
0.62	−2.51086	$4.16735\cdot10^2$	$-1.56012\cdot10^2$	0.9972	0.02
0.80	−3.26528	$6.96023\cdot10^2$	$-1.09573\cdot10^2$	0.9998	0.01
			K_2CO_3 15.0 wt%+2MPZ 5.0 wt%		
0.00	−2.83051	$5.40985\cdot10^2$	$-1.39457\cdot10^2$	0.9996	0.01
0.22	−1.81647	$2.13740\cdot10^2$	$-2.04578\cdot10^2$	0.9986	0.01
0.43	−1.80420	$2.25982\cdot10^2$	$-2.03485\cdot10^2$	1.0000	0.00
0.65	−1.57461	$1.86439\cdot10^2$	$-2.11059\cdot10^2$	0.9997	0.01
0.78	−1.84311	$2.55539\cdot10^2$	$-1.92101\cdot10^2$	0.9999	0.00
			K_2CO_3 15.0 wt%+2MPZ 7.0 wt%		
0.00	−4.14875	$1.09930\cdot10^3$	$-7.15696\cdot10$	0.9985	0.02
0.24	−2.34213	$3.96789\cdot10^2$	$-1.67745\cdot10^2$	0.9985	0.01
0.44	−2.36425	$3.89883\cdot10^2$	$-1.71826\cdot10^2$	0.9989	0.01
0.63	−1.67308	$2.15222\cdot10^2$	$-2.08579\cdot10^2$	0.9994	0.01
0.80	−1.81847	$2.60374\cdot10^2$	$-1.95884\cdot10^2$	0.9998	0.01
			K_2CO_3 15.0 wt%+2MPZ 7.5 wt%		
0.00	−7.14502	$3.05963\cdot10^3$	$9.00006\cdot10$	0.9992	0.01
0.23	−1.95300	$2.72878\cdot10^2$	$-1.98227\cdot10^2$	0.9996	0.01
0.41	−1.62486	$2.08420\cdot10^2$	$-2.10943\cdot10^2$	0.9998	0.00
0.63	−2.08170	$3.28967\cdot10^2$	$-1.82254\cdot10^2$	0.9997	0.01
0.74	−1.73273	$2.56526\cdot10^2$	$-1.95222\cdot10^2$	0.9979	0.02
			K_2CO_3 15.0 wt%+2MPZ 10.0 wt%		
0.00	−1.71549	$2.56121\cdot10^2$	$-2.03297\cdot10^2$	0.9999	0.00
0.20	−1.70882	$2.40338\cdot10^2$	$-2.08364\cdot10^2$	0.9992	0.01
0.40	−1.77180	$2.74438\cdot10^2$	$-1.97019\cdot10^2$	0.9999	0.00
0.60	−1.84255	$2.94963\cdot10^2$	$-1.92626\cdot10^2$	0.9997	0.01
0.71	−2.49590	$4.84907\cdot10^2$	$-1.57851\cdot10^2$	1.0000	0.00

calculated by Eq. (24) in Fig. 5. The density value was increased when the temperature increased constantly, and the slope of the regression curve was increased when the 2MPZ concentration increased.

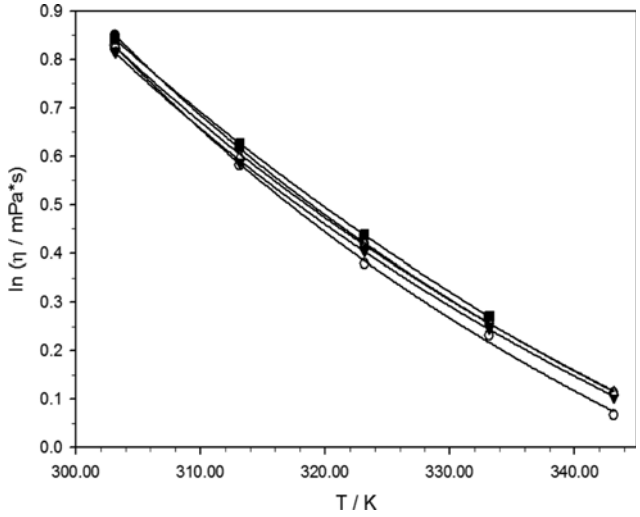

Fig. 6. Viscosity according to temperature K_2CO_3 15.0 wt%+2MPZ 10.0 wt%; ●, α=0; ○, α=0.20; ▼, α=0.40; △, α=0.60; ■, α=0.71; solid line, regression curve.

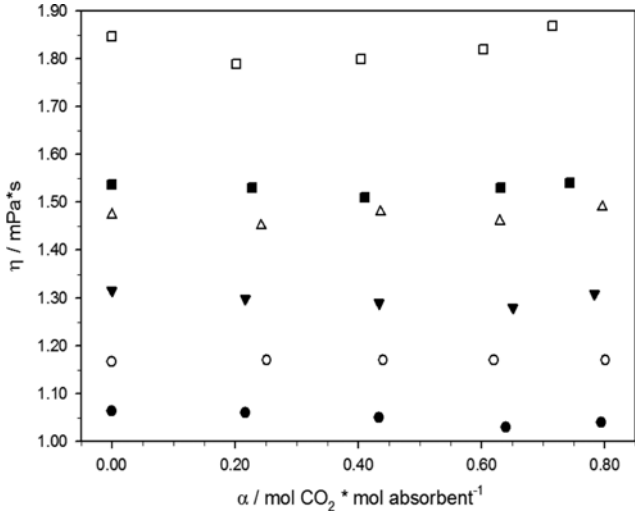

Fig. 7. Viscosity according to CO_2 loading of 313.15 K; ●, K_2CO_3 15.0 wt%+2MPZ 1.0 wt%; ○, K_2CO_3 15.0 wt%+2MPZ 3.0 wt%; ▼, K_2CO_3 15.0 wt%+2MPZ 5.0 wt%; △, K_2CO_3 15.0 wt%+2MPZ 7.0 wt%; ■, K_2CO_3 15.0 wt%+2MPZ 7.5 wt%; □, K_2CO_3 15.0 wt%+2MPZ 10.0 wt%.

4. Viscosity

The viscosities are presented in Table 6. Measured viscosities of pure CO_2-loaded absorbents were measured three times for each sample. The measured viscosity values showed relatively high repeatability (max SD=±0.04). The regression coefficient parameters of the viscosities can be expressed with Eq. (25) [35,36,38].

$$\eta/\text{mPa·s}=\exp[C_0+C_1(T/K+C_2)^{-1}] \quad (25)$$

(constant absorbent concentration)

The viscosity value decreased when the temperature increased constantly. The resulting values are presented in Table 7. The graph is shown with an example in Fig. 6. In conclusion, the viscosities decreased when the temperature increased at K_2CO_3 15.0 wt%+2MPZ 10.0 wt%.

The viscosity of the amine and blended amine solution (amine absorbent) was known to increase as the CO_2 loading increased. The viscosity of the amine absorbent increased by the increase in molecule interaction (formation of amine carbamate, protonated amine and bicarbonate). However, generally the increment of the viscosity is a large increment of the viscosity and is low when the concentration of the amine is low [9,42]. In this study, the concentration of 2MPZ is less than 10.0 wt%; therefore, the increment of viscosities was unclear when CO_2 was loaded in absorbent. The viscosity graph according to the CO_2 loading at 313.15 K is presented in Fig. 7.

5. Vapor Pressure

The vapor pressures are presented in Table 8. SDs appeared from the first decimal point. The vapor pressures have usually correlated well according to the Antoine equation [43,44].

The vapor pressure of the CO_2 absorbent correlated well with the Antoine equation, and this error is reported to be small [19, 27-29]. The Antoine equation is shown in Eq. (26):

Table 8. Experimental vapor pressure (P) for the CO_2-loaded aqueous K_2CO_3+2MPZ (wt%)

α/mol CO_2·mol solute^{-1}	P/kPa (SD)				
	303.15 K	313.15 K	323.15 K	333.15 K	343.15 K
			K_2CO_3 15.0 wt%+2MPZ 1.0 wt%		
0.00	3.9 (0.1)	6.8 (0.1)	11.4 (0.1)	18.6 (0.1)	29.2 (0.1)
0.22	4.0 (0.2)	7.0 (0.1)	11.8 (0.2)	19.0 (0.2)	29.7 (0.5)
0.43	5.1 (0.2)	8.7 (0.2)	14.3 (0.3)	22.6 (0.5)	34.6 (0.6)
0.64	8.2 (0.1)	13.7 (0.2)	21.9 (0.2)	33.5 (0.2)	49.5 (0.3)
0.79	11.6 (0.1)	19.6 (0.4)	31.1 (0.7)	46.8 (0.6)	-
			K_2CO_3 15.0 wt%+2MPZ 3.0 wt%		
0.00	3.8 (0.1)	6.6 (0.0)	11.2 (0.1)	18.3 (0.1)	28.8 (0.2)
0.25	3.9 (0.1)	6.9 (0.2)	11.6 (0.2)	18.9 (0.2)	29.6 (0.3)
0.44	5.0 (0.1)	8.6 (0.1)	14.2 (0.2)	22.6 (0.2)	34.9 (0.2)
0.62	8.0 (0.1)	13.4 (0.2)	21.6 (0.2)	33.3 (0.4)	49.8 (0.4)
0.80	11.7 (0.1)	19.5 (0.2)	30.7 (0.4)	46.6 (0.4)	-

Table 8. Continued

α/mol CO_2·mol solute^{-1}	P/kPa (SD)				
	303.15 K	313.15 K	323.15 K	333.15 K	343.15 K
			K_2CO_3 15.0 wt%+2MPZ 5.0 wt%		
0.00	3.8 (0.0)	6.6 (0.1)	11.2 (0.0)	18.1 (0.1)	28.6 (0.1)
0.22	3.9 (0.1)	6.8 (0.1)	11.4 (0.2)	18.4 (0.2)	28.8 (0.3)
0.43	4.9 (0.2)	8.3 (0.1)	13.8 (0.2)	22.2 (0.2)	34.5 (0.1)
0.65	8.8 (0.1)	14.5 (0.1)	23.2 (0.2)	35.9 (0.5)	53.9 (1.2)
0.78	12.1 (0.4)	19.7 (0.5)	30.7 (0.4)	46.8 (0.4)	-
			K_2CO_3 15.0 wt%+2MPZ 7.0 wt%		
0.00	3.8 (0.1)	6.6 (0.1)	11.1 (0.2)	18.1 (0.2)	28.4 (0.3)
0.24	3.8 (0.1)	6.6 (0.1)	11.3 (0.1)	18.4 (0.1)	28.9 (0.1)
0.44	4.6 (0.1)	8.0 (0.1)	13.4 (0.1)	21.7 (0.2)	34.1 (0.3)
0.63	7.9 (0.2)	13.2 (0.2)	21.4 (0.3)	33.7 (0.3)	51.1 (0.9)
0.80	12.2 (0.3)	20.0 (0.4)	31.4 (0.5)	47.8 (0.9)	-
			K_2CO_3 15.0 wt%+2MPZ 7.5 wt%		
0.00	3.7 (0.1)	6.5 (0.1)	10.9 (0.1)	17.9 (0.1)	28.0 (0.1)
0.23	3.8 (0.0)	6.7 (0.1)	11.2 (0.1)	18.3 (0.0)	28.8 (0.1)
0.41	4.5 (0.1)	7.8 (0.0)	13.1 (0.1)	21.4 (0.1)	33.4 (0.1)
0.63	8.1 (0.2)	13.6 (0.1)	22.0 (0.2)	34.7 (0.2)	53.3 (0.3)
0.74	11.1 (0.3)	18.3 (0.3)	28.9 (0.3)	44.5 (0.5)	-
			K_2CO_3 15.0 wt%+2MPZ 10.0 wt%		
0.00	3.6 (0.1)	6.4 (0.1)	10.7 (0.2)	17.5 (0.2)	27.6 (0.2)
0.20	3.6 (0.1)	6.5 (0.1)	10.9 (0.1)	17.8 (0.1)	27.9 (0.1)
0.40	4.3 (0.1)	7.5 (0.0)	12.7 (0.0)	20.7 (0.0)	32.8 (0.0)
0.60	7.4 (0.1)	12.5 (0.2)	20.6 (0.2)	32.7 (0.2)	50.6 (0.3)
0.71	10.5 (0.1)	17.8 (0.1)	28.5 (0.1)	44.1 (0.2)	-

$$P/kPa=\exp[D_0-D_1(T/K+D_2)^{-1}] \quad (26)$$
(constant absorbent concentration)

The regression coefficient parameters of the calculated vapor pressure are presented in Table 9. The R square and SEE are within acceptable error. An example of the correlated vapor pressure is shown in Fig. 8. Relationships between vapor pressure and CO_2 loading are shown in Eq. (27):

$$P/kPa=E_0+E_1(\alpha/CO_2 \text{ mol·amine mol}^{-1}) + E_2(\alpha/CO_2 \text{ mol·amine mol}^{-1})^2 + E_3(\alpha/CO_2 \text{ mol·amine mol}^{-1})^3 \text{ (constant temperature)} \quad (27)$$

The regression coefficient parameters, R squares and SEEs are presented in Table 10. The result of vapor pressure behavior is one

Table 9. Regressed parameters of vapor pressure (P) for temperature used in Eq. (26)

α/mol CO_2·mol solute^{-1}	Regression coefficient parameters				
	D_0	D_1	D_2	R^2	SEE
			K_2CO_3 15.0 wt%+2MPZ 1.0 wt%		
0.00	1.73848·10	$4.45771\cdot10^3$	−2.49617·10	1.0000	0.0
0.22	1.53531·10	$3.33311\cdot10^3$	−6.45137·10	1.0000	0.0
0.43	1.51651·10	$3.28537\cdot10^3$	−6.04403·10	1.0000	0.0
0.64	1.27861·10	$2.11102\cdot10^3$	$-1.05531\cdot10^2$	1.0000	0.0
0.79	1.06235·10	$1.19119\cdot10^3$	$-1.57394\cdot10^2$	1.0000	0.0
			K_2CO_3 15.0 wt%+2MPZ 3.0 wt%		
0.00	1.77982·10	$4.68450\cdot10^3$	−1.86413·10	1.0000	0.0
0.25	1.54263·10	$3.34232\cdot10^3$	−6.55109·10	1.0000	0.0
0.44	1.56608·10	$3.50348\cdot10^3$	−5.38119·10	1.0000	0.0
0.62	1.38000·10	$2.53576\cdot10^3$	−8.68065·10	1.0000	0.0
0.80	1.21797·10	$1.76108\cdot10^3$	$-1.21960\cdot10^2$	1.0000	0.0

Table 9. Continued

α/mol CO_2·mol solute^{-1}	Regression coefficient parameters				
	D_0	D_1	D_2	R^2	SEE
		K_2CO_3 15.0 wt%+2MPZ 5.0 wt%			
0.00	1.73822·10	4.45906·10^3	−2.53006·10	1.0000	0.0
0.22	1.61463·10	3.78231·10^3	−4.73351·10	1.0000	0.0
0.43	1.89993·10	5.50366·10^3	1.29326·10	1.0000	0.0
0.65	1.62436·10	3.80266·10^3	−3.28761·10	1.0000	0.0
0.78	1.54265·10	3.32630·10^3	−4.59452·10	1.0000	0.0
		K_2CO_3 15.0 wt%+2MPZ 7.0 wt%			
0.00	1.75752·10	4.58928·10^3	−2.05800·10	1.0000	0.0
0.24	1.69146·10	4.15043·10^3	−3.68055·10	1.0000	0.0
0.44	1.73733·10	4.38100·10^3	−2.66978·10	1.0000	0.0
0.63	1.67825·10	4.04474·10^3	−2.83108·10	1.0000	0.0
0.80	1.43355·10	2.72318·10^3	−7.30304·10	1.0000	0.0
		K_2CO_3 15.0 wt%+2MPZ 7.5 wt%			
0.00	1.65629·10	3.98457·10^3	−4.19475·10	1.0000	0.0
0.23	1.66424·10	4.01833·10^3	−4.06185·10	1.0000	0.0
0.41	1.74847·10	4.44726·10^3	−2.48851·10	1.0000	0.0
0.63	1.82708·10	4.91285·10^3	5.19483·10^{-1}	1.0000	0.0
0.74	1.55686·10	3.35126·10^3	−4.85151·10	1.0000	0.0
		K_2CO_3 15.0 wt%+2MPZ 10.0 wt%			
0.00	1.60634·10	3.70588·10^3	−5.24181·10	1.0000	0.0
0.20	1.40348·10	2.67270·10^3	−9.35459·10	1.0000	0.0
0.40	1.82197·10	4.85794·10^3	−1.33270·10	1.0000	0.0
0.60	1.82225·10	4.82264·10^3	−5.85843	1.0000	0.0
0.71	1.30292·10	2.06558·10^3	−1.09692·10^2	1.0000	0.0

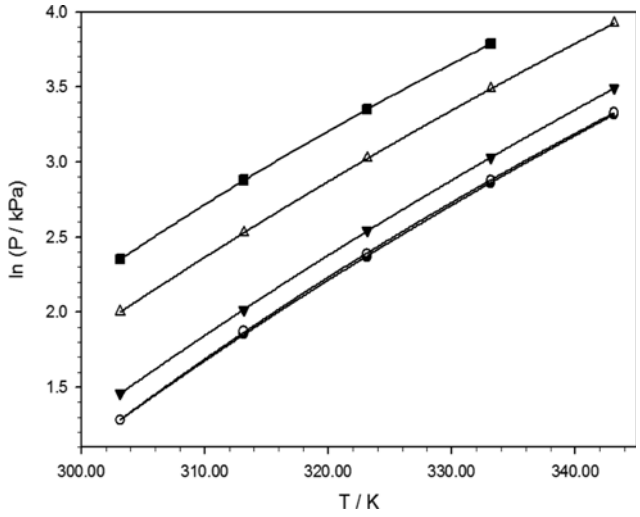

Fig. 8. Vapor pressure according to temperature of K_2CO_3 15.0 wt%+2MPZ 10.0 wt%; ●, α=0.20; ○, α=0; ▼, α=0.40; △, α=0.60; ■, α=0.71; solid line, regression curve.

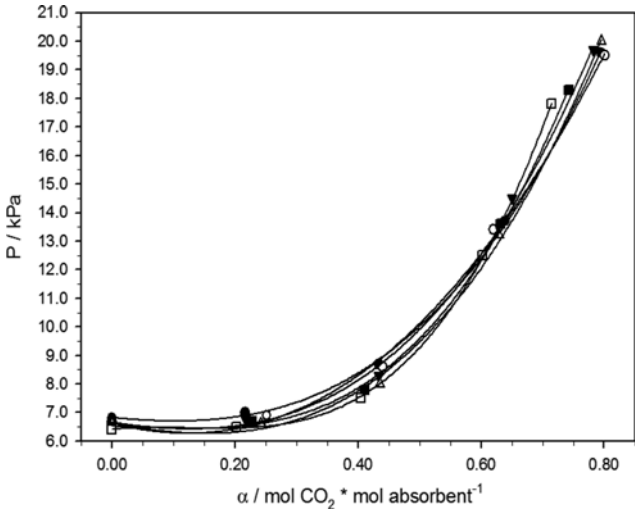

Fig. 9. Vapor pressure according to CO_2 loading of 313.15 K; ●, K_2CO_3 15.0 wt%+2MPZ 1.0 wt%; ○, K_2CO_3 15.0 wt%+2MPZ 3.0 wt%; ▼, K_2CO_3 15.0 wt%+2MPZ 5.0 wt%; △, K_2CO_3 15.0 wt%+2MPZ 7.0 wt%; ■, K_2CO_3 15.0 wt%+2MPZ 7.5 wt%; □, K_2CO_3 15.0 wt%+2MPZ 10.0 wt%; solid line, regression curve.

that is generally observed when CO_2 gas is mixed in an aqueous solution of a basic compound [45-50]. Chemically, CO_2 is absorbed in an absorbent solution at low CO_2 loading, but some CO_2 is physically dissolved at high CO_2 loading [48].

Behaviors between CO_2 gas and the basic component in an aqueous solution are shown in Fig. 9. Changes in the vapor pressure are not observed when CO_2 is completely chemically absorbed at a

Table 10. Regressed parameters of vapor pressure (P) for CO_2 loading used in Eq. (27)

K_2CO_3+2MPZ/ wt%	Regression coefficient parameters					
	E_0	E_1	E_2	E_3	R^2	SEE
			303.15 K			
15.0+1.0	3.91764	−2.12885	8.18050	8.46489	0.9993	0.2
15.0+3.0	3.82168	−4.50884	1.68487·10	1.41328	0.9980	0.3
15.0+5.0	3.83058	−2.22276	6.23682	1.30550·10	0.9982	0.3
15.0+7.0	3.82266	−2.52086	4.28980	1.53155·10	0.9958	0.3
15.0+7.5	3.71323	$-3.34922\cdot10^{-1}$	−3.49387	2.34340·10	0.9994	0.2
15.0+10.0	3.60847	$1.04338\cdot10^{-1}$	−7.50823	2.92337·10	0.9998	0.1
			313.15 K			
15.0+1.0	6.82344	−2.07268	6.86681	2.02125·10	0.9995	0.2
15.0+3.0	6.63509	−5.73819	2.22250·10	6.37693	0.9980	0.5
15.0+5.0	6.65278	−3.20875	8.63397	2.16742·10	0.9979	0.5
15.0+7.0	6.63165	−4.20671	8.53506	2.25893·10	0.9988	0.4
15.0+7.5	6.52511	$-6.54438\cdot10^{-1}$	−4.44014	3.60836·10	0.9991	0.3
15.0+10.0	6.41099	2.18799	−2.12408·10	5.67009·10	0.9994	0.1
			323.15 K			
15.0+1.0	1.14350·10	−1.79043	5.21847	3.56233·10	0.9996	0.3
15.0+3.0	1.12572·10	−9.88139	3.80170·10	6.00905	0.9977	0.8
15.0+5.0	1.12839·10	−6.88001	2.15662·10	2.45786·10	0.9975	0.9
15.0+7.0	1.11572·10	−6.07510	1.48028·10	3.14150·10	0.9983	0.7
15.0+7.5	1.09392·10	−2.66081	2.47271	4.56131·10	0.9991	0.5
15.0+10.0	1.07228·10	1.81726	−2.25478·10	7.68363·10	0.9994	0.0
			333.15 K			
15.0+1.0	1.86460·10	−3.59891	9.11958	5.05520·10	0.9996	0.5
15.0+3.0	1.83829·10	−1.36922·10	5.22573·10	1.13508·10	0.9977	1.2
15.0+5.0	1.82139·10	−1.05601·10	3.59307·10	3.15036·10	0.9979	1.2
15.0+7.0	1.81932·10	−1.15404·10	3.46771·10	3.38059·10	0.9979	1.2
15.0+7.5	1.79617·10	−6.74834	1.79493·10	5.32847·10	0.9990	0.8
15.0+10.0	1.75442·10	$4.76475\cdot10^{-1}$	−2.12530·10	$1.01848\cdot10^{2}$	0.9996	0.5
			343.15 K			
15.0+1.0	2.92000·10	2.65814	−2.58530·10	$1.11833\cdot10^{2}$	1.0000	0.0
15.0+3.0	2.88000·10	5.34131	−4.58582·10	$1.48184\cdot10^{2}$	1.0000	0.0
15.0+5.0	2.86000·10	$8.90449\cdot10^{-1}$	−2.88502·10	$1.34111\cdot10^{2}$	1.0000	0.0
15.0+7.0	2.84000·10	5.11008	−5.12212·10	$1.59681\cdot10^{2}$	1.0000	0.0
15.0+7.5	2.80000·10	7.35288	−5.56501·10	$1.70203\cdot10^{2}$	1.0000	0.0
15.0+10.0	2.76000·10	4.80966	−5.27322·10	$1.79309\cdot10^{2}$	1.0000	0.0

low CO_2 loading less than 0.25. The vapor pressure curve is changed at high CO_2 loading over 0.25.

CONCLUSIONS

The physical properties of the aqueous K_2CO_3+2MPZ solution were investigated at 303.15-343.15 K. The density, viscosity, and vapor pressure were measured under various absorbent concentrations and CO_2 loadings. An experimental formula was obtained from the regression analysis of the data plots. The regression coefficient parameters with high reliability of measured physical properties were calculated. The density values increased when the concentration increased and when the CO_2 loading increased. The regression coefficient parameters of the measured densities facilitate the prediction of the physical properties.

The viscosity values increased as the concentration increased, and the viscosity values decreased when the temperature increased. However, viscosity changes were not indicated when CO_2 loadings increased because the 2MPZ concentration was low.

The vapor pressure of CO_2 absorbent was applied using the Antoine equation. The vapor pressure behavior of CO_2-loaded absorbents indicated vapor pressure change between the CO_2 gas and a basic component in an aqueous solution. The vapor pressure curve changed at CO_2 loading over 0.25.

ACKNOWLEDGEMENTS

This work was supported by the Energy Demand Management

Technology Program of the Korea Institute of Energy Technology Evaluation and Planning (KETEP), granted financial resource from the Ministry of Trade, Industry and Energy, Republic of Korea. (No. 20152010201940)

REFERENCES

1. A. Bello and R. O. Idem, *Ind. Eng. Chem. Res.*, **45**, 2569 (2006).
2. M. Wang, A. Lawal, P. Stephenson, J. Sidders and C. Ramshaw, *Chem. Eng. Res. Des.*, **89**, 1609 (2011).
3. G. Astarita, *Mass transfer with chemical reaction*, Elsevier (1967).
4. R. Baker and D. McCrea, *The Benfield LOHEAT process: an improved HPC absorption process*, in Presented at AIChE 1981 Spring National Meeting, Houston TX (1981).
5. R. Bartoo, *Chem. Eng. Prog.*, **80**, 35 (1984).
6. R. Bartoo, T. Gemborys and C. Wolf, *Recent improvements to the benfield process extend its use*, in Nitrogen'91 Conference (1991).
7. S. Furukawa and R. Bartoo, *Improved Benfield process for ammonia plants*, Universal Oil Products, Des Plaines, IL, USA (1997).
8. Y. I. Yoon, Y. E. Kim, S. C. Nam, S. K. Jeong, S. Y. Park, M. H. Youn and K. T. Park, *Energy Procedia*, **63**, 1745 (2014).
9. T. G. Amundsen, L. E. Øi and D. A. Eimer, *J. Chem. Eng. Data*, **54**, 3096 (2009).
10. R. H. Weiland, J. C. Dingman, D. B. Cronin and G. J. Browning, *J. Chem. Eng. Data*, **43**, 378 (1998).
11. T. Sherwood, G. Shipley and F. Holloway, *Ind. Eng. Chem.*, **30**, 765 (1938).
12. Y. Zhang, H. Chen, C.-C. Chen, J. M. Plaza, R. Dugas and G. T. Rochelle, *Ind. Eng. Chem. Res.*, **48**, 9233 (2009).
13. S. Mirzaei, A. Shamiri and M. K. Aroua, *Rev. Chem. Eng.*, **31**, 521 (2015).
14. J. H. Choi, S. G. Oh, M. Jo, Y. I. Yoon, S. K. Jeong and S. C. Nam, *Chem. Eng. Sci.*, **72**, 87 (2012).
15. O. Gorset, J. N. Knudsen, O. M. Bade and I. Askestad, *Energy Procedia*, **63**, 6267 (2014).
16. G. Rochelle, E. Chen, S. Freeman, D. Van Wagener, Q. Xu and A. Voice, *Chem. Eng. J.*, **171**, 725 (2011).
17. D. Singh, E. Croiset, P. L. Douglas and M. A. Douglas, *Energy Convers. Manage.*, **44**, 3073 (2003).
18. L. M. Romeo, I. Bolea and J. M. Escosa, *Appl. Therm. Eng.*, **28**, 1039 (2008).
19. K. Khimeche, F. Djellouli, A. Dahmani and I. Mokbel, *Chem. Eng. Data*, **56**, 4972 (2011).
20. D. Sanyal, N. Vasishtha and D. N. Saraf, *Ind. Eng. Chem. Res.*, **27**, 2149 (1988).
21. K. Smith, G. Xiao, K. Mumford, J. Gouw, I. Indrawan, N. Thanumurthy, D. Quyn, R. Cuthbertson, A. Rayer and N. Nicholas, *Energy Fuels*, **28**, 299 (2013).
22. G. Astarita, D. W. Savage and J. M. Longo, *Chem. Eng. Sci.*, **36**, 581 (1981).
23. J. Han, J. Jin, D. A. Eimer and M. C. Melaaen, *J. Chem. Eng. Data*, **57**, 1095 (2012).
24. Y. Maham, T. T. Teng, L. G. Hepler and A. E. Mather, *J. Solution Chem.*, **23**, 195 (1994).
25. Y. Maham, C. N. Liew and A. Mather, *J. Solution Chem.*, **31**, 743 (2002).
26. U. S. Arachchige, N. Aryal, D. A. Eimer and M. C. Melaaen, *Ann. T. Nord. Rheol. Soc.*, **21**, 299 (2013).
27. A. Belabbaci, A. Razzouk, I. Mokbel, J. Jose and L. Negadi, *J. Chem. Eng. Data*, **54**, 2312 (2009).
28. I. Kim, H. F. Svendsen and E. Børresen, *J. Chem. Eng. Data*, **53**, 2521 (2008).
29. S. H. Wu, A. R. Caparanga, R. B. Leron and M. H. Li, *Exp. Therm Fluid Sci.*, **48**, 1 (2013).
30. H. Svensson, C. Hulteberg and H. T. Karlsson, *Energy Procedia*, **63**, 750 (2014).
31. F. C. Riesenfeld and A. L. Kohl, *Gas purification*, Gulf Publishing Company (1974).
32. Y. E. Kim, J. H. Choi, S. C. Nam and Y. I. Yoon, *J. Ind. Eng. Chem.*, **18**, 105 (2012).
33. Y. E. Kim, S. H. Yun, J. H. Choi, S. C. Nam, S. Y. Park, S. K. Jeong and Y. I. Yoon, *Energy Fuels*, **29**, 2582 (2015).
34. G. T. Rochelle, G. Goff, T. Cullinane and S. Freguia. *Research results for CO_2 capture from flue gas by aqueous absorption/stripping*, in Proceedings of the Laurance Reid Gas Conditioning Conference (2002).
35. J. H. Song, S. B. Park, J. H. Yoon, H. Lee and K. H. Lee, *J. Chem. Eng. Data*, **41**, 1152 (1996).
36. S. Lee, S. I. Choi, S. Maken, H. J. Song, H. C. Shin, J. W. Park, K. R. Jang and J. H. Kim, *J. Chem. Eng. Data*, **50**, 1773 (2005).
37. Y. Geng, S. Chen, T. Wang, D. Yu, C. Peng, H. Liu and Y. Hu, *J. Mol. Liq.*, **143**, 100 (2008).
38. Y. Zhao, X. Zhang, S. Zeng, Q. Zhou, H. Dong, X. Tian and S. Zhang, *J. Chem. Eng. Data*, **55**, 3513 (2010).
39. H. J. Song, M. G. Lee, H. Kim, A. Gaur and J. W. Park, *J. Chem. Eng. Data*, **56**, 1371 (2011).
40. G. Murshid, A. M. Shariff, L. K. Keong and M. A. Bustam, *J. Chem. Eng. Data*, **56**, 2660 (2011).
41. S. A. Jayarathna, A. Weerasooriya, S. Dayarathna, D. A. Eimer and M. C. Melaaen, *J. Chem. Eng. Data*, **58**, 986 (2013).
42. D. Fu, L. Chen and L. Qin, *Fluid Phase Equilib.*, **319**, 42 (2012).
43. C. Antoine, *CR Hebd. Séances Acad. Sci.*, **107**, 681 (1888).
44. G. W. Thomson, *Chem. Rev.*, **38**, 1 (1946).
45. R. Gibbons and A. Laughton, *Fluid Phase Equilib.*, **18**, 61 (1984).
46. R. Stryjek and J. Vera, *Fluid Phase Equilib.*, **25**, 279 (1986).
47. B. T. Brandes, *Ind. Eng. Chem Res.*, **44**, 639 (2005).
48. Á. Pérez-Salado Kamps, E. Meyer, B. Rumpf and G. Maurer, *J. Chem. Eng. Data*, **52**, 817 (2007).
49. M. B. Shiflett, D. J. Kasprzak, C. P. Junk and A. Yokozeki, *J. Chem. Thermodyn.*, **40**, 25 (2008).
50. G. Kuranov, B. Rumpf, N. A. Smirnova and G. Maurer, *Ind. Eng. Chem. Res.*, **35**, 1959 (1996).